Deep inelastic neutron scattering from fluid para- and orthohydrogen

1998 J. Phys.: Condens. Matter 10 7091

(http://iopscience.iop.org/0953-8984/10/32/002)

J. Phys.: Condens. Matter **10** (1998) 7091–7111. Printed in the UK PII: S0953-8984(98)93393-8

Deep inelastic neutron scattering from fluid para- and orthohydrogen

C Andreani†, D Colognesi†, A Filabozzi†, E Pace‡ and M Zoppi§

† Dipartimento di Fisica e Istituto Nazionale di Fisica della Materia, Università di Roma 'Tor Vergata', Via della Ricerca Scientifica 1, 00133 Rome, Italy

‡ Dipartimento di Fisica e Istituto Nazionale di Fisica Nucleare, Università di Roma 'Tor Vergata', Via della Ricerca Scientifica 1, 00133 Rome, Italy

§ Consiglio Nazionale delle Ricerche, Istituto di Elettronica Quantistica, Via Panciatichi 56/30, 50127 Florence, Italy

Received 14 April 1998, in final form 2 June 1998

Abstract. New experimental neutron scattering data from fluid and solid molecular hydrogen at high momentum transfer are interpreted by means of a theoretical calculation able to describe the data both for parahydrogen and for an ortho-parahydrogen mixture over a wide momentum transfer range. Our approach, valid for any diatomic molecule, reveals the occurrence of final state effects in the scaling function and their q dependence. It appears that at high momentum transfer the dominant final state effects are those coming from the intramolecular interaction.

1. Introduction

In recent years, owing to the availability of an intense flux of electronvolt neutrons at pulsed neutron sources, the experimental technique of *deep inelastic neutron scattering* (DINS), has demonstrated its potential for providing unique and detailed information about the mean kinetic energy and single-particle momentum distribution in a variety of classical and quantum systems. As a consequence a well established user program now exists in various areas of neutron science, i.e. quantum fluids, molecular science, hydrogen bonds, atomic and molecular hydrogen in materials, and an established community of users routinely employing this technique [1]. DINS is analogous to the measurement of electron momentum distributions by Compton scattering [2] or the measurement of nucleon momentum distributions by electron scattering from nuclei [3]: the whole set of techniques rely on the assumption that the momentum distribution of target particles (electrons, nucleons or atoms) can be obtained by inelastic scattering of the high-energy incident probes (photons, electrons or neutrons, respectively). These techniques also share the basic principles of data interpretation, based on the validity of the *impulse approximation* (IA) [4], which is supposed to hold in the limit of high values of both energy $\hbar\omega$, and momentum $\hbar q$, transferred by the probe to the target, as was shown to be the case for square integrable and for harmonic interactions [5, 6]. Indeed, within the IA assumption, the scattering cross section can be described by means of a scaling variable y [7], and a scaling function $F(y, q)$ which for $q \to \infty$, approaches an asymptotic value $F(y)$, independent of q, determined by the momentum distribution.

In the case of inelastic neutron scattering from diatomic molecular fluids at low values of momentum transfer, neutrons are scattered from the whole molecule, while, as q increases,

0953-8984/98/327091+21$19.50

one obtains scattering off the single nuclei in the molecule. One can easily calculate the values of the momentum transfer which yield scattering from a single nucleus by means of the incoherent condition $q \gg 2\pi/r_0$, where r_0 is the molecular bond length. More accurately, the incoherent limit is reached when $f_1(q) = 1$, with $f_1(q)$ being the intramolecular static form factor [8]. For H_2, this condition is surely well satisfied for $q > 30$ Å^{-1}. Indeed it has already been shown experimentally in recent papers [9, 10] that for these values of momentum transfer, the ω and q values at the maximum of the cross section are linked by the relation $\omega = \hbar q^2/2M$, where M is the proton mass and not the molecule mass. Generally speaking one can expect that IA holds when the energy transfer is much higher than the typical vibrational excitation energy of the molecule (516 meV in H_2) and it is well known that deviations from the IA asymptotic scattering regime occur at the large, but finite, q values available in a real neutron experiment. These deviations are referred to as *final state effects* (FSE) [11] and arise from the interaction of the recoiling single particle with the rest of the system. For systems composed of monatomic species only one sort of FSE is present, which is the result of the interaction of the struck particle with its environment through the intermolecular potential. In the following these effects will be referred to as *intermolecular final state effects* (INTERFSE). For a diatomic or polyatomic system, in addition to the aforementioned effects, FSE also come from the interaction of the scattered atom with the other atoms within the same molecule (*intramolecular final state effects*: INTRAFSE). At low q (5 Å$^{-1} < q < 20$ Å^{-1}) INTRAFSE are generally interpreted by studying the excited states of the rotovibrational structure of the molecule [12, 13]. As a general result the presence of both kinds of FSE determines asymmetries in the measured $F(y, q)$ and clear shifts of its maximum position from $y = 0$. Although it is generally well accepted that these asymmetries and shifts become smaller as q increases, the debate about the size and form of FSE in quantum fluids and the extent to which they affect $F(y, q)$ is still an open question.

In previous papers a model independent procedure has been proposed for deriving the asymptotic response function and the momentum distributions in molecular systems [14] and a theoretical model has been proposed to describe the scattering function of diatomic molecules at $q \to \infty$ [10, 15, 16].

In this paper we will present an extension of our work aimed at describing the scattering process from diatomic molecules in the DINS regime at intermediate q values (30 Å$^{-1} < q < 60$ Å^{-1}), where the asymptotic regime has not yet been reached. We will compare the result of our calculation with new experimental DINS data on solid and fluid H_2 in a wider thermodynamic regime than in previous experiments [10]. In order to reach a better experimental resolution, besides the routinely used Au filter, a U filter has been employed to determine the energy of the scattered neutrons on the eVS spectrometer. In section 2 we present our theoretical framework for a diatomic system. The experiment and the data analysis are described in section 3, while section 4 is devoted to the comparison with theoretical calculations and to discussion. Section 5 contains the conclusions.

2. Theoretical background: DINS at intermediate Q values

In previous papers [10, 15] we have obtained the asymptotic scaling function of diatomic molecular fluids by approximating the final-state wavefunctions with plane waves and neglecting $1/q$ terms in the δ function in the limit $q \to \infty$. Our aim is to obtain a theoretical expression for the scaling function able to follow the behaviour of the experimental data at finite intermediate values of q, where the asymptotic limit has not yet been reached. The final states will be still described as plane waves, while the $1/q$ terms in the energy

conserving δ function will be taken care of in an approximate way, generalizing an approach proposed by Stringari for liquid ^{4}He [17] to the case of a molecular diatomic fluid. A brief note of the results obtained has already been published [16].

Let us treat homonuclear diatomic molecular fluids as statistical mixtures of different thermally excited levels. We will not consider high-temperature fluids, where electronic excitations and dissociations become likely. The inelastic differential cross-section at high energy and momentum transfer for neutron scattering from diatomic molecules can be written as follows

$$\frac{\mathrm{d}^2\sigma}{\mathrm{d}\Omega\,\mathrm{d}E'} = \frac{K_f}{K_i}\sum_{I,F} P_I \left|\langle\Phi_F|\sum_{n=1}^{2}\hat{b}_n \exp(\mathrm{i}\boldsymbol{q}\cdot\boldsymbol{r}_n)|\Phi_I\rangle\right|^2 \delta(\hbar\omega + E_I - E_F). \tag{1}$$

In (1), K_i and K_f are the initial and final wavevectors of the scattered neutron, E' is its final energy, Φ_I and Φ_F are the initial and final-state wavefunctions for a single molecule in the fluid system, E_I and E_F are the corresponding initial and final energies, P_I the statistical weights of the initial states, $\hat{b}_1 = \hat{b}_2 \equiv \hat{b}$ the scattering operators for the nuclei 1 and 2, and $\boldsymbol{r}_n$ ($n = 1, 2$) the coordinates of the nuclei. The initial and the final-state wavefunctions can be decomposed into orbital $\Psi_{i(f)}$, and spinorial $\chi_{i'(f')}$, parts. The initial and final energies E_I and E_F are independent of the spinorial degrees of freedom and then can be labelled as E_i and E_f. Let us consider the inelastic structure factor

$$S(q,\omega) = \frac{K_i}{2K_f}\left(\frac{\mathrm{d}^2\sigma}{\mathrm{d}\Omega\,\mathrm{d}E'}\right)\frac{1}{\langle|b|^2\rangle} \tag{2}$$

where $\langle|b|^2\rangle = \sum_{i',f'} g_{i'}|\langle\chi_{f'}|\hat{b}|\chi_{i'}\rangle|^2$ with $g_{i'}$ the inverse of the spin multiplicity of the incident neutron and of the nuclei 1 and 2 [15]. In the incoherent approximation, i.e. neglecting the interference terms owing to the high momentum transfer, the inelastic structure factor becomes

$$S(q,\omega) = \sum_i p_i \sum_f |\langle\Psi_f|\exp(\mathrm{i}\boldsymbol{q}\cdot\boldsymbol{r}_1)|\Psi_i\rangle|^2\delta(\hbar\omega + E_i - E_f) \tag{3}$$

where p_i are the statistical weights which refer to the orbital states. In the absence of strong intermolecular forces, the initial state energy is the sum of a translational term E_m and of an internal energy term $E_{v,j}$ ($E_i = E_m + E_{v,j}$), and the initial wavefunction in (3) can be written as follows: $\Psi_i(\boldsymbol{r},\boldsymbol{R}) = \phi_{v,j,m_j}(\boldsymbol{r})\psi_m(\boldsymbol{R})$, where $\phi_{v,j,m_j}(\boldsymbol{r})$ describes the relative motion of the two nuclei and $\psi_m(\boldsymbol{R})$ describes the motion of the centre of mass of a single molecule in the bulk. The coordinate $\boldsymbol{R} = (\boldsymbol{r}_1 + \boldsymbol{r}_2)/2$ is the coordinate of the centre of mass of the molecule and $\boldsymbol{r} = \boldsymbol{r}_1 - \boldsymbol{r}_2$ is the relative coordinate. An analogous factorization of the wavefunction will be used for the final state $\Psi_f(\boldsymbol{r},\boldsymbol{R}) = \phi_r(\boldsymbol{r})\psi_g(\boldsymbol{R})$ and the final energy will be rewritten as a sum of a translational term E_g, and an internal energy term E_r; $E_f = E_g + E_r$, where g and r represent the translational and the internal quantum numbers of the final state, respectively. Since in its initial state, H_2 is in a Σ electronic ground state, the relative wavefunction can be decomposed into radial and angular functions as follows

$$\phi_{v,j,m_j}(\boldsymbol{r}) = \frac{1}{r}u_{v,j}(r)Y_{j,m_j}(\hat{r}) \tag{4}$$

where $u_{v,j}(r)$ describes the vibrational motion of the nuclei and $Y_{j,m_j}(\hat{r})$ is the angular wavefunction. Using the relation $E_i = E_m + E_{v,j}$, the statistical weight can also be factorized into centre of mass p_m, and internal $p_{v,j}$, weights

$$p_i = p_m p_{v,j}. \tag{5}$$

Then we can write

$$S(q,\omega)=\sum_{r,g}\sum_{v,j,m_j}p_{v,j}\sum_{m}p_m|\langle\psi_g|\exp(\mathrm{i}\boldsymbol{q}\cdot\boldsymbol{R})|\psi_m\rangle|^2|\langle\phi_r|\exp(\mathrm{i}\boldsymbol{q}\cdot\boldsymbol{r}/2)|\phi_{v,j,m_j}\rangle|^2 \times\delta(\hbar\omega+E_m+E_{v,j}-E_r-E_g). \tag{6}$$

Let us introduce the intermediate scattering function $I(q,t)$ as follows

$$I(q,t)=\hbar\int_{-\infty}^{\infty}\exp(\mathrm{i}\omega t)S(q,\omega)\,\mathrm{d}\omega=I_{CM}(q,t)\sum_{v,j}p_{v,j}I_{v,j}(q,t) \tag{7}$$

where

$$I_{CM}(q,t)=\sum_{g}\sum_{m}p_m|\langle\psi_g|\exp(\mathrm{i}\boldsymbol{q}\cdot\boldsymbol{R})|\psi_m\rangle|^2\exp\left(\frac{\mathrm{i}}{\hbar}(E_g-E_m)t\right) \tag{8}$$

and

$$I_{v,j}(q,t)=\sum_{r}\sum_{m_j=-j}^{j}\left|\langle\phi_r|\exp\left(\mathrm{i}\boldsymbol{q}\cdot\frac{\boldsymbol{r}}{2}\right)|\phi_{v,j,m_j}\rangle\right|^2\exp\left(\frac{\mathrm{i}}{\hbar}(E_r-E_{v,j})t\right) \tag{9}$$

represent the intermolecular and intramolecular intermediate scattering functions, respectively. As will be shown in the following, within the *plane wave approximation* (PWA) one can express these two functions in terms of the momentum distributions for the intermolecular and intramolecular motion separately.

Stringari [17] proposed the introduction, in the energy conserving δ function of the structure factor (3), a constant average potential energy in addition to the kinetic energy in order to take into account, at least in an approximate way, the interaction between the struck particle and the rest of the system in the final state. This approach was able to explain the shift of the maximum of the scaling function with respect to the pure IA in the case of liquid ^{4}He. In the following we will generalize this approach to the case of diatomic molecular fluids considering two distinct average potential energies, one for the interaction of the struck molecule in the fluid, and another for the interaction between the nuclei in this molecule. As will be shown in section 4, the shape of the structure factor is essentially determined by the dynamics of the internal modes of the molecule, while the centre-of-mass dynamics of the molecule only slightly affects $S(q,\omega)$.

Let us consider the intermolecular contribution first. Assuming the PWA, we have the following expressions for the centre-of-mass final state ψ_g, and its energy eigenvalue E_g

$$\psi_g(\boldsymbol{R})=\frac{1}{\sqrt{8\pi^3}}\exp(\mathrm{i}\boldsymbol{K}\cdot\boldsymbol{R}) \tag{10}$$

$$E_g=\frac{\hbar^2}{4M}K^2+\langle V_g\rangle \tag{11}$$

where M is the mass of a single atom of the diatomic molecule and $\langle V_g\rangle$ is an approximate, constant and independent of g (i.e. of $\boldsymbol{K}$), average value for the intermolecular interaction acting on the final states of the centre-of-mass wavefunction. The sum over g in (8) has to be replaced by an integral in $\mathrm{d}\boldsymbol{K}$, and then the intermolecular intermediate scattering function becomes

$$I_{CM}(q,t)=\sum_{m}p_m\frac{1}{8\pi^3}\int\mathrm{d}\boldsymbol{K}|\langle\exp[\mathrm{i}(\boldsymbol{q}-\boldsymbol{K})\cdot\boldsymbol{R}]|\psi_m\rangle|^2\exp\left[\mathrm{i}\left(\frac{\hbar}{4M}K^2+\frac{\langle V_g\rangle}{\hbar}-\frac{E_m}{\hbar}\right)t\right] \simeq\int N(\boldsymbol{K}-\boldsymbol{q})\exp\left[\mathrm{i}\left(\frac{\hbar}{4M}K^2+\frac{\langle V_g\rangle}{\hbar}-\frac{\overline{E_m}}{\hbar}\right)t\right]\mathrm{d}\boldsymbol{K} \tag{12}$$

where in the last step of the previous equation, the centre-of-mass energy E_m has been replaced by a constant value $\overline{E_m}$. The function $N(\boldsymbol{P})$ is the momentum distribution of the centre of mass of the molecule in the bulk

$$N(\boldsymbol{P}) = \sum_m p_m \left| \int \mathrm{d}\boldsymbol{R} \frac{\exp(-\mathrm{i}\boldsymbol{P}\cdot\boldsymbol{R})}{\sqrt{8\pi^3}} \psi_m(\boldsymbol{R}) \right|^2. \tag{13}$$

In quantum molecular fluids (hydrogen and deuterium at high density and low temperature), a Gaussian shape of $N(\boldsymbol{P})$ is considered a reasonable description [18]

$$N(\boldsymbol{P}) = \frac{1}{\sqrt{8\pi^3}\sigma_T^3} \exp\left(\frac{-|\boldsymbol{P}|^2}{2\sigma_T^2}\right) \tag{14}$$

where σ_T is simply related to the mean value of the kinetic energy of the centre of mass, averaged over the initial states ψ_m weighted by p_m, $\langle\overline{T_m}\rangle$, through the following equation

$$\sigma_T = \sqrt{4M\langle\overline{T_m}\rangle/(3\overline{\hbar}^2)}. \tag{15}$$

The variance σ_T^2 is related to the temperature T in a complex way and has a finite value even at $T = 0$, i.e. there is a zero-point value of $\langle\boldsymbol{P}^2\rangle$ (and then of $\langle\overline{T_m}\rangle$), other than zero. By increasing the temperature and by lowering the density the classic regime is reached, where $\langle\overline{T_m}\rangle = 3/2\ k_B T$.

In order to satisfy the *first moment sum rule*, we assume in (12): $\langle V_g\rangle \equiv \langle\overline{V_m}\rangle = \overline{E_m} - \langle\overline{T_m}\rangle$ (see the appendix), where $\langle\overline{V_m}\rangle$ is the mean value of the potential energy of the centre of mass, averaged over all the initial states ψ_m weighted by p_m, as for $\langle\overline{T_m}\rangle$. After the substitution $\boldsymbol{P} = \boldsymbol{K} - \boldsymbol{q}$, $I_{CM}(q,t)$ becomes

$$I_{CM}(q,t) = \int N(\boldsymbol{P}) \exp\left[\mathrm{i}\left(\frac{\overline{\hbar}}{4M}q^2 + \frac{\overline{\hbar}}{4M}P^2 + \frac{\overline{\hbar}}{2M}\boldsymbol{P}\cdot\boldsymbol{q} - \frac{\langle\overline{T_m}\rangle}{\overline{\hbar}}\right)t\right]\mathrm{d}\boldsymbol{P}. \tag{16}$$

Let us now consider the intramolecular contribution that comes from the internal structure of the molecule. In the PWA [5, 6, 19], the intramolecular final state wavefunctions and eigenvalues can be cast as

$$\phi_r(\boldsymbol{r}) = \frac{1}{\sqrt{8\pi^3}} \exp(\mathrm{i}\boldsymbol{k}\cdot\boldsymbol{r}) \tag{17}$$

$$E_r = \frac{\overline{\hbar}^2}{M}k^2 + \langle V_r\rangle \tag{18}$$

where $\langle V_r\rangle$ is an approximate, constant and independent of r (i.e. of $\boldsymbol{k}$), mean value for the intramolecular interaction acting on the final states internal wavefunctions. The sum over r in (9) has to be replaced by an integral in $\mathrm{d}\boldsymbol{k}$, and then the intramolecular intermediate scattering function becomes

$$\begin{aligned} I_{v,j}(q,t) &= \frac{1}{(2j+1)} \sum_{m_j=-j}^{j} \frac{1}{8\pi^3} \int \mathrm{d}\boldsymbol{k} |\langle \exp[\mathrm{i}(\boldsymbol{q}/2 - \boldsymbol{k})\cdot\boldsymbol{r}] | \phi_{v,j,m_j}\rangle|^2 \\ &\quad \times \exp\left[\frac{\mathrm{i}}{\overline{\hbar}}\left(\frac{\overline{\hbar}^2}{M}k^2 + \langle V_r\rangle - E_{v,j}\right)t\right] \\ &= \int n_{v,j}(\boldsymbol{k} - \boldsymbol{q}/2) \exp\left[\frac{\mathrm{i}}{\overline{\hbar}}\left(\frac{\overline{\hbar}^2}{M}k^2 + \langle V_r\rangle - E_{v,j}\right)t\right]\mathrm{d}\boldsymbol{k} \end{aligned} \tag{19}$$

where $n_{v,j}(\boldsymbol{p})$ is the square of the Fourier transform of the wavefunction of the relative motion in the initial state, $\phi_{v,j,m_j}(\boldsymbol{r})$, averaged over m_j, i.e. the internal momentum distribution for the state v, j

$$n_{v,j}(\boldsymbol{p}) = \frac{1}{2j+1}\sum_{m_j=-j}^{j}\left|\int \mathrm{d}\boldsymbol{r}\frac{\exp(-\mathrm{i}\boldsymbol{p}\cdot\boldsymbol{r})}{\sqrt{8\pi^3}}\phi_{v,j,m_j}(\boldsymbol{r})\right|^2. \tag{20}$$

We assume that $\phi_{v,j,m_j}(\boldsymbol{r})$ of the H_2 molecule in the initial state is well described by the ideal harmonic approximation, i.e. that molecular rotations are ideal and completely decoupled from vibrations, centrifugal distortions are neglected, and vibrations are purely harmonic. This is a good approximation for the initial states which are relevantly populated in the low temperature range in which we are interested in (see the following section), i.e. $v = 0$, $j = 0, 1$. As a consequence $n_{v,j}(\boldsymbol{p})$ is given by

$$n_{v,j}(\boldsymbol{p}) = \frac{\alpha}{2^{v+1}\sqrt{\pi^5}v!}\left|\int_0^\infty r\; j_j(pr)\exp\left(-\frac{\alpha^2}{2}(r-r_o)^2\right)H_v[\alpha(r-r_o)]\,\mathrm{d}r\right|^2 \tag{21}$$

where H_v are the Hermite polynomials, j_j the spherical Bessel functions, and α is directly connected to the vibrational frequency of the molecules, ω_o ($\alpha^2 = \mu\omega_o/\hbar$, $\hbar\omega_o = 516$ meV for the H_2 molecule [20]), while r_o ($r_o = 0.742$ Å^{-1} in the H_2 molecule [20]) and μ are the bond length and reduced mass of the molecule, respectively. Within the same ideal harmonic approximation, the internal statistical weight of (7), $p_{v,j}$, can be calculated using the expression

$$p_{v,j} = \frac{(2j+1)c_j\exp[-(E_v+E_j)/(K_BT)]}{Z} \tag{22}$$

with E_v as the vibrational energy, E_j the rotational energy, Z a normalization constant and c_j the nuclear spinorial degeneration factor. In the case of H_2, c_j has only two values: one for odd j ($c_{2n+1} = 3$) and another for even j ($c_{2n} = 1$) [20].

For the intramolecular potential energy, as for the intermolecular one, we assume $\langle V_r\rangle \equiv \langle V_{v,j}\rangle = E_{v,j} - \langle T_{v,j}\rangle$ (see the appendix), where $\langle V_{v,j}\rangle$ is the mean value, independent of m_j, of the intramolecular potential energy in the initial state ϕ_{v,j,m_j}, and $\langle T_{v,j}\rangle$ is the corresponding mean value of the intramolecular kinetic energy. After the substitution: $\boldsymbol{p} = \boldsymbol{k} - \boldsymbol{q}/2$, $I_{v,j}(q,t)$ becomes

$$I_{v,j}(q,t) = \int n_{v,j}(\boldsymbol{p})\exp\left[\mathrm{i}\left(\frac{\hbar}{4M}q^2 + \frac{\hbar}{M}p^2 + \frac{\hbar}{M}\boldsymbol{p}\cdot\boldsymbol{q} - \frac{\langle T_{v,j}\rangle}{\hbar}\right)t\right]\mathrm{d}\boldsymbol{p}. \tag{23}$$

Let us consider the scaling variable y

$$y = \frac{M}{\hbar^2 q}\left(\hbar\omega - \frac{\hbar^2q^2}{2M}\right) \tag{24}$$

and the scaling function

$$F(y,q) = \frac{\hbar^2 q}{M}S(q,\omega). \tag{25}$$

It is quite useful to introduce the Fourier transform of $F(y,q)$, i.e. $\tilde{F}(s,q)$

$$\tilde{F}(s,q) = \int_{-\infty}^{\infty}\exp(\mathrm{i}sy)F(y,q)\,\mathrm{d}y. \tag{26}$$

It is worth noting that $\tilde{F}(s,q)$ is simply related to $I(q,t)$ by means of a phase factor

$$\tilde{F}(s,q) = \exp\left(-\mathrm{i}\frac{sq}{2}\right)I(q,t) \tag{27}$$

where s has the meaning of the distance covered by the recoiling nucleus at time t

$$s = \frac{\overline{h}}{M} q t. \tag{28}$$

It is also clear that $\tilde{F}(s,q)$ can be decomposed in centre of mass, $\tilde{F}_{CM}(s,q)$, and intramolecular factors

$$\tilde{F}(s,q) = \tilde{F}_{CM}(s,q) \sum_{v,j} p_{v,j} \tilde{F}_{v,j}(s,q) \tag{29}$$

where

$$\tilde{F}_{CM}(s,q) = \exp\left(-\mathrm{i}\frac{sq}{4}\right) I_{CM}(q,t) \tag{30}$$

and

$$\tilde{F}_{v,j}(s,q) = \exp\left(-\mathrm{i}\frac{sq}{4}\right) I_{v,j}(q,t). \tag{31}$$

Using the well known convolution theorem, a more compact way of writing the scaling function appears

$$F(y,q) = \sum_{v,j} p_{v,j} \int_{-\infty}^{\infty} F_{v,j}(y-y',q) F_{CM}(y',q)\ dy' \tag{32}$$

with

$$F_{v,j}(y,q) = \frac{1}{2\pi} \int_{-\infty}^{\infty} \exp(-\mathrm{i}sy) \tilde{F}_{v,j}(s,q)\,\mathrm{d}s \tag{33}$$

$$F_{CM}(y,q) = \frac{1}{2\pi} \int_{-\infty}^{\infty} \exp(-\mathrm{i}sy) \tilde{F}_{CM}(s,q)\,\mathrm{d}s. \tag{34}$$

In terms of the momentum distributions, by choosing the z axis in the direction of $\boldsymbol{q}$, one obtains

$$F_{v,j}(y,q) = \int n_{v,j}(\boldsymbol{p}) \delta\left(y - p_z - \frac{p^2}{q} + \frac{M}{\overline{h}^2 q} \langle T_{v,j} \rangle\right) \mathrm{d}\boldsymbol{p} \tag{35}$$

and

$$F_{CM}(y,q) = \int N(\boldsymbol{P}) \delta\left(y - \frac{P_z}{2} - \frac{P^2}{4q} + \frac{M}{\overline{h}^2 q} \langle \overline{T_m} \rangle\right) \mathrm{d}\boldsymbol{P}. \tag{36}$$

It is easy to check that for $q \to \infty$ the $1/q$ dependent terms in (35) and (36) disappear and the asymptotic scaling function in IA is recovered [10, 15].

Before comparing the theoretical expression for the scaling function with the experimental data, a convolution of $F(y,q)$ with the experimental resolution function has to be performed. This yields

$$F_R^{th}(y,q) = \int F(y',q) R(y-y',q)\,\mathrm{d}y'. \tag{37}$$

Table 1. Parameters describing the resolution function $R(y)$, for the mass $M = 1.0079$ amu, at the scattering angles of the experimental data for both Au and U foils. In the first case $R(y)$ is well represented by a Voigt function, while in the second, a Gaussian function is adequate. The geometrical component of $R(y)$ is well described by a Gaussian function of standard deviation σ_G for both foils. On the contrary, the energy contribution to the resolution function is represented by a Lorentzian function in the case of Au foil ($\Gamma_E/2$ is the HWHM of this Lorentzian) and by a Gaussian function in that of the U foil (σ_E is the standard deviation of this Gaussian). At each angle the momentum transfer $\bar{q}$, corresponding to the maximum of each recoil peak, is also shown.

#	$2\theta^\circ$	$\bar{q}$ (Å^{-1})	σ_G (Å^{-1})	$\Gamma_E/2$ (Å^{-1})	Foil
16	50.1	58.2	0.70	0.63	Au
15	48.2	54.5	0.71	0.66	Au
14	46.1	50.6	0.72	0.71	Au
13	44.1	47.2	0.72	0.76	Au
12	42.1	44.0	0.72	0.82	Au
11	40.0	40.8	0.72	0.88	Au
10	37.9	38.0	0.73	0.94	Au
9	35.9	35.2	0.73	1.01	Au
#	$2\theta^\circ$	$\bar{q}$ (Å^{-1})	σ_G (Å^{-1})	σ_E (Å^{-1})	Foil
25	42.4	51.8	0.77	0.30	U
26	40.5	48.4	0.77	0.32	U
27	38.6	45.4	0.77	0.34	U
28	36.8	42.4	0.78	0.36	U
29	34.9	39.7	0.78	0.39	U
30	33.0	36.9	0.78	0.42	U
31	31.2	34.3	0.78	0.45	U
32	29.3	31.8	0.79	0.48	U

3. DINS experiment on H_2

The experiment was performed at the *neutron spallation source* ISIS, operating at the Rutherford Appleton Laboratory (UK), and employed the eVS spectrometer, an inverse geometry instrument, using an incident pulsed neutron beam with energies in the range 1–100 eV [21].

The energies of the scattered neutrons were determined by using resonance absorption filters (both uranium and gold foils) fixed on an aluminium frame and placed between the sample and the scintillation detectors. Foils are moved in and out of the scattered neutron beam cyclically every 300 s. This procedure of data recording allows the effect of possible drifts in the efficiency of the detectors during a single run to be averaged out. The measurements presented here were obtained by using gold filters, with an absorption resonance energy of 4911 meV [22], and uranium filters, with an absorption resonance energy of 6671 meV [22]. The energies and energy widths of the nuclear resonances were checked by measurements of the scattering from a Pb standard sample. The scattering angles 2θ, of each of 9–16 (Au foil) and 25–32 (U foil) detectors which we used in this experiment and the corresponding momentum transfers are reported in table 1.

Five independent contributions to resolution function $R(y)$, arise from uncertainties in the following instrument components: neutron time-of-flight, initial and final flight paths, scattering angles and energy values of the analyser foil. Therefore $R(y)$ on eVS depends on both the geometrical configuration of the instrument (this component is well described

Table 2. Thermodynamic conditions for experimental data, specified by temperature, T, molecular density ρ, state S, and percentage of parahydrogen of the sample. IC is the total integrated proton current of each run and σ_T the standard deviation related to the translational kinetic energy of the H_2 molecule (15). The averaged values for σ_T, $IC \cdot \rho$ and parahydrogen percentage are also reported for the summed runs A–D and E–I.

#	T (K)	ρ (nm^{-3})	State	Para. (%)	σ_T (Å^{-1})	IC (μA h)
A	10	26.45	S	100.0	1.450	3381
B	17	22.41	L	99.9	1.341	4052
C	30	22.41	L	97.0	1.476	4570
D	40	22.41	G	88.7	1.578	3902
E	50	22.41	G	77.1	1.690	3333
F	60	22.41	G	65.6	1.792	3588
G	48	10.45	G	79.4	1.503	1912
H	70	10.45	G	56.0	1.771	6065
I	110	10.45	G	35.8	2.182	2024

Sum	Para. (%)	$\overline{\sigma_T}$ (Å^{-1})	$IC \cdot \rho$ (μA h nm^{-3})
A–D	96.2	1.467	3.695×10^5
E–I	65.3	1.768	2.596×10^5

by a Gaussian function) and on the intrinsic energy width of the resonance foil. The latter includes two distinct contributions: a Gaussian one, coming from the thermal vibrations of the lattice constituting the metallic foil, and a Lorentzian-like one, coming from the Breit–Wigner absorption cross section of the nuclei [23]. In the case of Au foil, the contribution coming from the lattice is small and can be included in the main Lorentzian component, so that the only Gaussian contribution to $R(y)$ comes from the geometrical component, giving rise to an overall Voigt function shape for $R(y)$. On the contrary, for U foil, the Breit–Wigner contribution is almost negligible in comparison with the lattice one and the overall $R(y)$ is well approximated by a Gaussian function [24]. The total resolution components for each detector are reported in table 1, where σ_G is the standard deviation of the geometrical components, while σ_E represent the standard deviation of the intrinsic Gaussian component of the U foil and $\Gamma_E/2$ is the *half width at half maximum* (HWHM) for the intrinsic Lorentzian component of the Au foil.

The sample was very high purity hydrogen (quoted as 99.999% pure) placed within two coaxial aluminium tubes separated by a 1.0 mm gap. This cylindrical sample holder was coupled to the cold finger of a closed circuit helium 'Orange' cryostat and connected to the external gas handling system by means of a $1/16''$ OD stainless steel tube. A hydrogen sample was measured in nine different thermodynamic conditions (see table 2), namely at three different densities: $\rho = 26.45$ molecules nm^{-3} at 10 K; $\rho = 22.41$ molecules nm^{-3} at five temperatures between 17 and 60 K; $\rho = 10.45$ molecules nm^{-3} at three temperatures between 48 and 110 K. At these temperatures different equilibrium percentages of parahydrogen ($j = 0$) and orthohydrogen ($j = 1$) are present in our sample (see table 2). For all temperatures the statistical weights $p_{j=2}$ are not greater than the same statistical weight $p_{j=2}$ at $T = 110$ K (i.e. $p_{j=2} \leqslant 1.6 \times 10^{-2}$). Therefore the analysis was carried out considering that only the initial states $j = 0$ and $j = 1$ are populated. The equilibrium conditions can be reached starting from room temperature ordinary gas only if the sample is cooled in the presence of specific catalytic paramagnetic salts (solid Cr_2O_3–γAl_2O_3) [25], that were placed at the bottom of the cell, out of the incident beam.

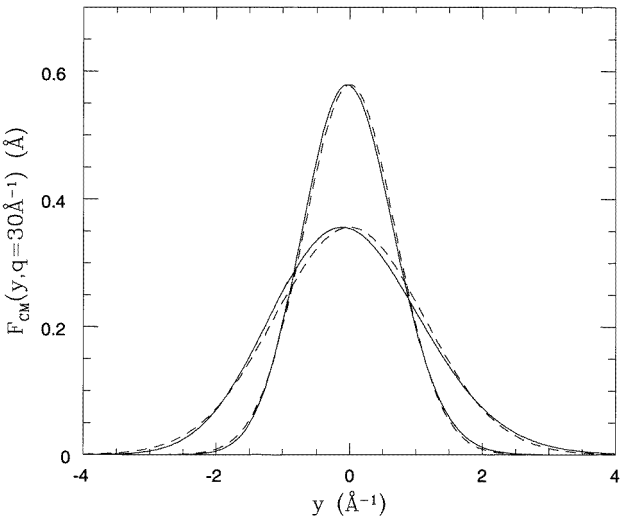

Figure 1. $F_{CM}(y,q)$ for $q = 30$ Å^{-1} is plotted as full curves at two temperatures, $T = 17$ K (narrow peak) and $T = 110$ K (broad peak). The mean kinetic energies for these two states are respectively 64.3 and 171.8 K and both exceed the classical values. The broken curves represent the corresponding asymptotic scaling function $F_{CM}(y)$.

The thermodynamic conditions were continuously monitored throughout the experiment by checking the temperature and pressure in the sample container. At each thermodynamic point three runs, lasting 12 h each, were performed and were subsequently summed together, after checking the stability of the whole system. For each measurement the total integrated current of the proton accelerator, IC, obtained in this way is reported in table 2. Experimental data reduction was performed for each detector and thermodynamic condition separately: the filter-in and filter-out time-of-flight spectra were normalized to the monitor detector and then subtracted off. In this way the fast neutron background is also removed from data. The subtraction of cell contribution was not necessary, because hydrogen and aluminium recoil peaks are placed at different positions in eVS time-of-flight spectra. Multiple scattering was evaluated by means of a Monte Carlo routine, and its intensity was found to be completely negligible in comparison with primary scattering. Subsequently, time-of-flight data have been transformed in y–q space using standard eVS routines, choosing the mass of a single hydrogen atom ($M_H = 1.0079$ amu) as recoil mass (see section 2).

As was anticipated in section 2, the centre-of-mass dynamics of the molecule described by $F_{CM}(y,q)$ (see (36)), which is strongly dependent on temperature and density through the mean kinetic energy (see σ_T in table 2), does contribute very little to the scaling function of the system. This can be appreciated from figure 1, where $F_{CM}(y,q)$ is shown for state B ($T = 17$ K and $\rho = 22.41$ nm^{-3}) and state I ($T = 110$ K and $\rho = 10.45$ nm^{-3}), at $q = 30$ Å^{-1} and from figure 2, where for the state B the whole $F(y,q)$ function (from (29)) is compared with $\sum_{v,j} p_{v,j} F_{v,j}(y,q)$ (being for this state mainly $v = 0$ and $j = 0$, see table 2). In figures 1 and 2 we have also reported the corresponding asymptotic functions calculated in the IA limit ($q \to \infty$). From figure 1 we observe a negligible shift towards negative values of y of the scaling function at $q = 30$ Å^{-1} and a strong dependence on σ_T, but with a HWHM which is in any case only of the order of ~ 1 Å^{-1}. This finding explains why in figure 2 the widths and the shifts of the broken and full curves are nearly

the same. As a consequence we can conclude that most of the shift of the peak and HWHM of $F(y,q)$ at $q = 30$ Å^{-1} are due, in figure 2, to the contributions coming from $F_{v,j}(y,q)$. Since the same kind of behaviour is also observed for all temperatures, we can conclude that temperature influences the total $F(y,q)$ essentially through $p_{v,j}$. For this reason, in order to increase the statistical accuracy, data sets A–D containing essentially parahydrogen (an average orthohydrogen percentage of less than 4%) on one side, and data sets E–I, containing a mixture of ortho- and parahydrogen (orthohydrogen percentage on average $\simeq$35%) on the other, have been summed together, properly weighted with $IC \cdot \rho$. This procedure was adopted for data recorded from both U (summing the responses from the states A–D and E–I for the individual detectors 25–32) and Au (summing the responses from the states A–D and E–I for the individual detectors 9–16) foils, yielding at each scattering angle only two averaged scaling functions $F_R^{\exp}(y,q)$. In the following the sum for the states A–D will be referred to as *parahydrogen* and the sum for the states E–I as *mixture*. We observed that the averaged data for parahydrogen with the gold foil are almost equal to the data corresponding to the thermodynamic states A, B, C and D.

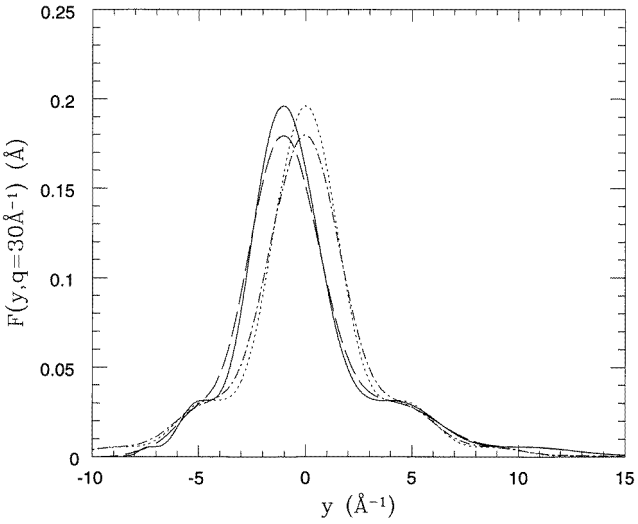

Figure 2. $F(y,q)$ for $q = 30$ Å^{-1} at $T = 17$ K (broken curve), $F_{v,j}(y,q)$ ($v = 0$, $j = 0$) (full curve), and the corresponding asymptotic scaling function $F(y)$ (chain curve) and $F_{v,j}(y)$ (dotted curve).

4. Data analysis and discussion

In order to compare experimental data and the theoretical calculations described in section 2, the theoretical scaling function $F_R^{th}(y,q)$ (see (37)) has been calculated at a fixed scattering angle for the exact values of the y–q space covered by each detector using the corresponding resolution function $R(y)$, constructed with the parameter listed in table 1. In this way a $F_R^{th}(y,q)$ for each detector has been produced. In the calculation of $F_R^{th}(y,q)$ we have used $\hbar\omega_o = 516$ meV for the vibrational frequency, $r_o = 0.742$ Å for the molecular bond length [20] (see (21)), while $\langle \bar{T}_m \rangle$ is derived from σ_T through (18) and $\langle T_{v=0,j=0} \rangle = 129$ meV and $\langle T_{v=0,j=1} \rangle = 144$ meV.

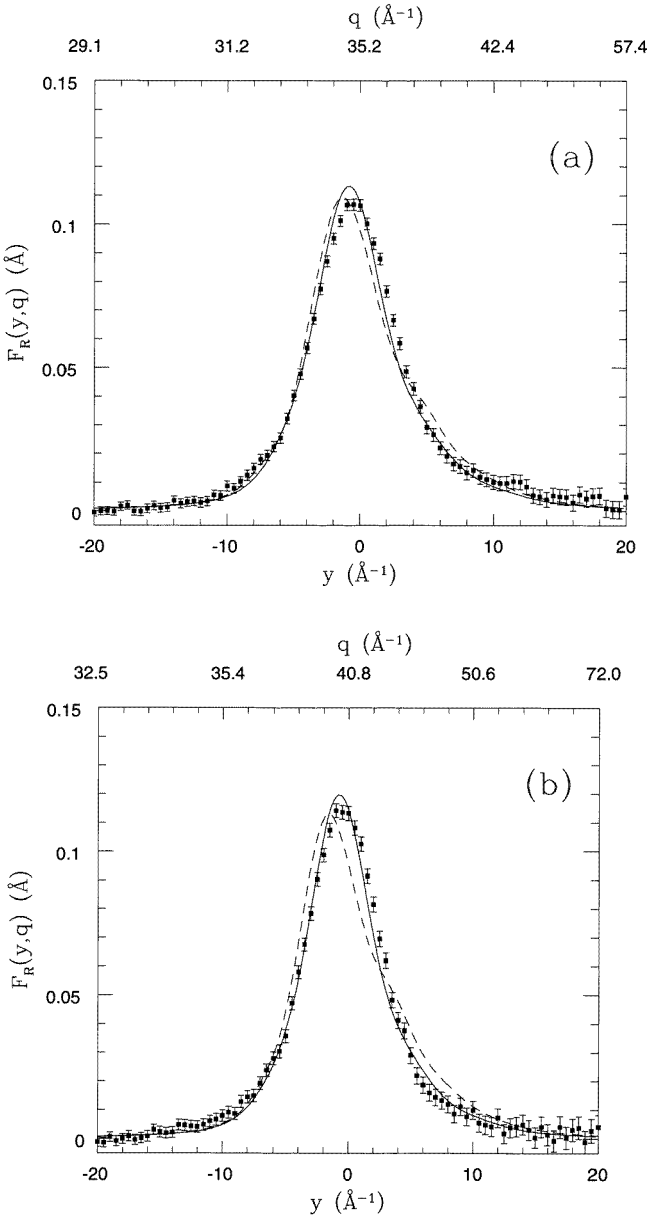

Figure 3. Experimental $F_R^{\exp}(y,q)$ (full squares) for *parahydrogen* (A–D states and Au foil, see text) and $\bar{F}_R^{th}(y,q)$ (full curve) for four scattering angles, $2\theta = 35.9^\circ$, 40.0°, 44.1° and 50.1°, are plotted in (a), (b), (c) and (d), respectively. The lower abscissa is the scaling variable y, and the top abscissa the momentum transfer q. In (a) and (b) the theoretical scaling function obtained from Young and Koppel model $\bar{F}_{(YK)R}^{th}(y,q)$, is also plotted (short-dashed curve), while in (d) we include the asymptotic scaling function $\bar{F}_R^{th}(y)$, (long-dashed curve).

The calculations of $F_R^{th}(y,q)$ involved a convolution with the intermolecular $F_{CM}(y,q)$ according to (29) and (36), where $N(P)$ is a Gaussian molecular momentum distribution (14). For each thermodynamic state we calculated σ_T (see (15)) using

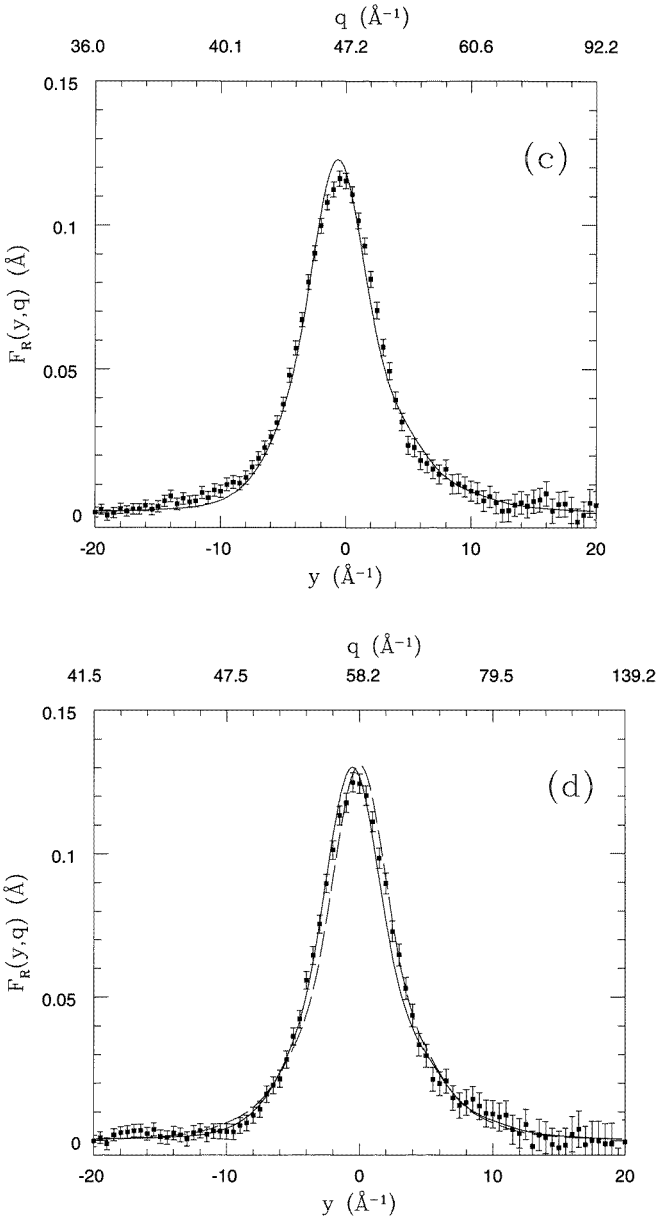

Figure 3. (Continued)

a *path integral Monte Carlo* simulation (PIMC) [26], a well assessed technique for determining the macroscopic and microscopic properties of quantum systems [27], fluid parahydrogen included [28]. In particular the calculated σ_T values for parahydrogen agree very well, within statistical accuracy, with those derived from a previous experiment performed on the MARI spectrometer on fluid H_2 [26], in the same thermodynamic conditions. Our results obtained from PIMC simulations are reported in table 2.

In the same way as for the experimental $F_R^{\exp}(y,q)$, only two averaged $\bar{F}_R^{th}(y,q)$ have been considered: one for the *parahydrogen* and one for the *mixture*, summing the responses corresponding to the states A–D and E–I with the proper values for IC and statistical weights.

In figures 3(a)–(d) a comparison between experimental scattering data $F_R^{\exp}(y,q)$ from *parahydrogen* using Au foil and $\bar{F}_R^{th}(y,q)$, calculated for the corresponding scattering angles, is shown, while in figures 4(a) and (b) the comparison is between $\bar{F}_R^{th}(y,q)$ and experimental parahydrogen data using U foil. The experimental data were normalized by introducing a constant for each detector and performing a fit relative to the theoretical results in the range -15 Å$^{-1} \leqslant y \leqslant 15$ Å^{-1} for Au foil and -10 Å$^{-1} \leqslant y \leqslant 15$ Å^{-1} for the U foil. In the latter case, owing to a small inconsistency in the energy value derived from the resonant foil, a small shift of the peak position has been allowed in the range (0.0 ± 0.5) Å^{-1}. A similar procedure has been set up for data coming from the *mixture*. Figures 5(a)–(d) show a comparison between experimental scattering data from the *mixture* (Au foil) and $\bar{F}_R^{th}(y,q)$, calculated for each scattering angle and broadened for the proper resolution function $R(y)$, while in figures 6(a) and (b) the comparison is established between the *mixture* (U foil) and $\bar{F}_R^{th}(y,q)$ treated in the same way as before. The reduced χ^2 values obtained for these four sets of data are shown in table 3. A satisfactory agreement is obtained between calculations and experiment in the four sets of data in the whole q range, especially as far as the *mixture* is concerned. From these figures we observe that our theory describes DINS scattering quite well as a function of q and that, as expected, the agreement is certainly more satisfactory for data obtained at the highest values of q in particular for the Au foil. For completeness, at the highest q values (figures 3(d) and 5(d)) the scattering response in the asymptotic limit, $F(y)$, has also been plotted. The values of χ^2 for *parahydrogen* ($\chi^2 = 2.71$) and for the *mixture* ($\chi^2 = 1.23$) obtained in this case demonstrate that the final state effects are not yet negligible even at the highest experimental q value of 58 Å^{-1}.

Table 3. Values for reduced χ^2 as determined from the fits on experimental data for *parahydrogen* (A–D states) and *mixture* (E–I states) using our calculation or the Young and Koppel (YK) model. Detectors 9–16 are for the Au foil and detectors 25–32 for the U foil.

#	χ^2 (Para.)	χ^2 (Para.)(YK)	χ^2 (Mix.)	χ^2 (Mix.)(YK)	$\bar{q}$ (Å^{-1})
16	1.00	—	0.45	—	58.2
15	1.95	—	1.12	—	54.5
14	1.70	—	0.84	—	50.6
13	2.05	—	1.17	—	47.2
12	1.86	—	1.27	—	44.0
11	2.11	11.6	1.34	4.90	40.8
10	2.19	7.97	1.24	3.47	38.0
9	2.79	7.45	1.17	3.05	35.2
#	χ^2 (Para.)	χ^2 (Para.)(YK)	χ^2 (Mix.)	χ^2 (Mix.)(YK)	$\bar{q}$ (Å^{-1})
25	2.02	—	1.61	—	54.0
26	1.49	—	0.72	—	51.5
27	1.37	—	0.74	—	49.2
28	0.90	—	0.71	—	47.0
29	1.97	—	1.24	—	44.9
30	2.14	4.21	0.87	2.32	42.8
31	2.25	3.73	0.92	1.99	40.9
32	1.66	2.53	0.79	1.39	39.0

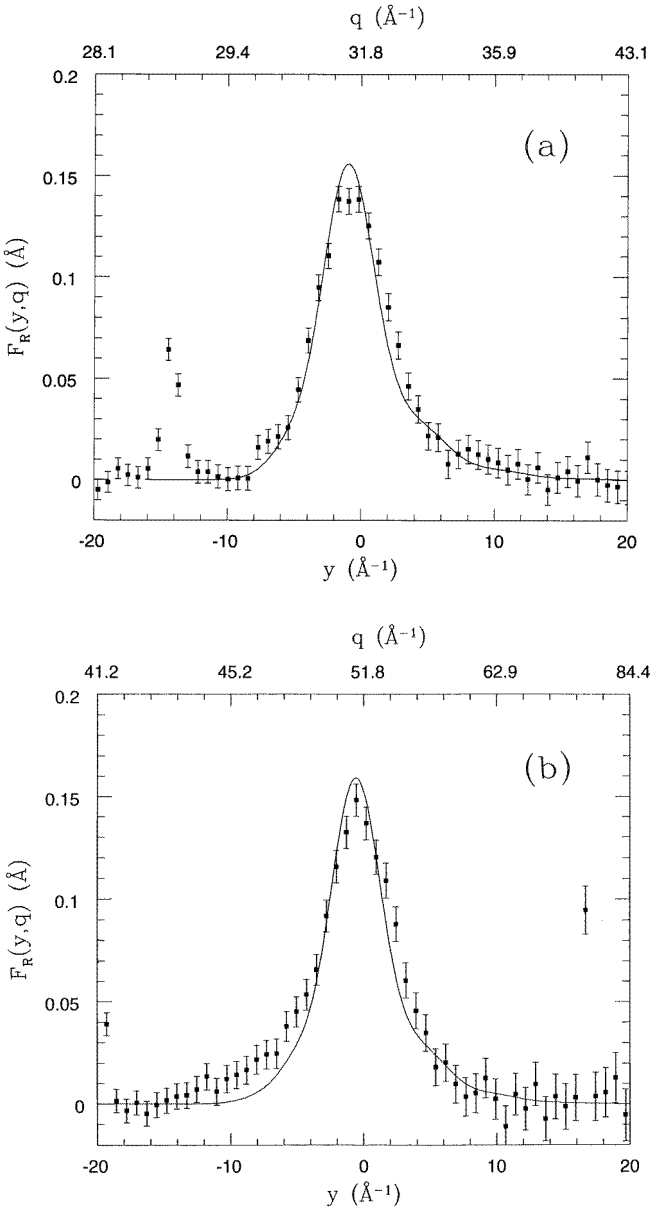

Figure 4. Experimental $F_R^{\exp}(y,q)$ (full squares) for *parahydrogen* (A–D states and U foil, see text) and $\bar{F}_R^{th}(y,q)$ (full curve) for two scattering angles, $2\theta = 29.3^\circ$ and 42.4°, are plotted in (a) and (b), respectively. The lower abscissa is the scaling variable y, and the top abscissa the momentum transfer q. The spurious peaks are the cell contributions produced by the different uranium resonances (left side 6671 meV, right side 20 872 meV).

Furthermore we have attempted to explain the departures from the IA using, for the description of the final states in the intramolecular scaling function, the simple free rotator model proposed by Young and Koppel (YK) [13]. This model is expected to describe the experimental data for those values of energy transfer to the intramolecular

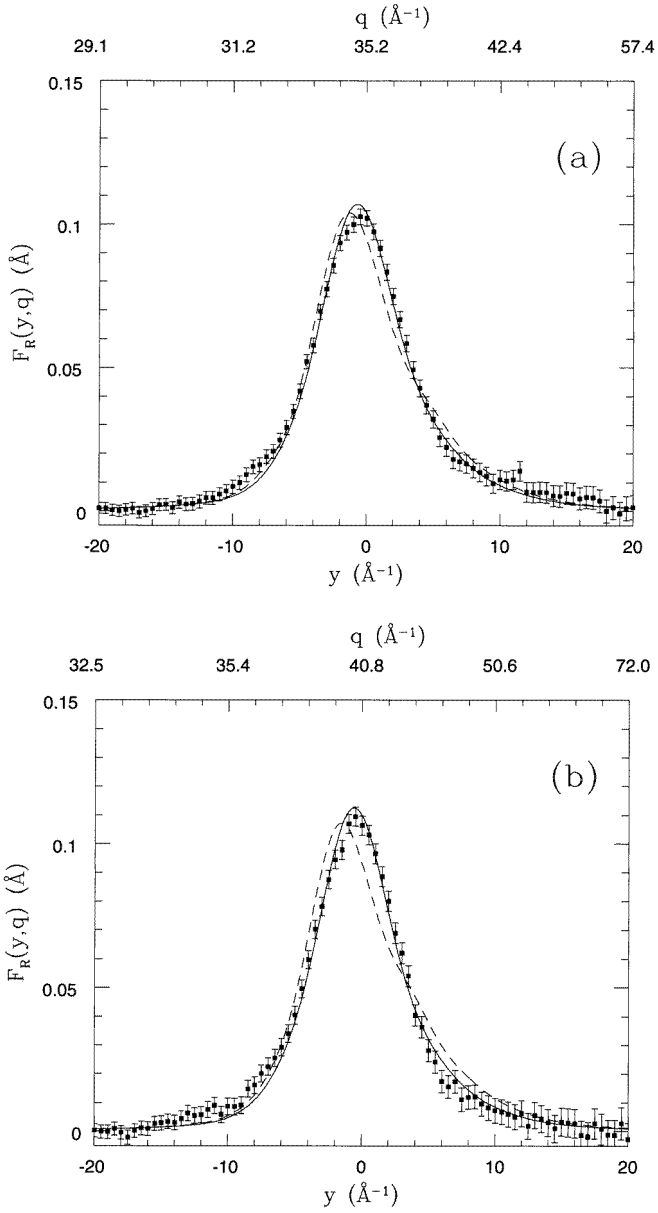

Figure 5. Experimental $F_R^{\exp}(y, q)$ (full squares) for *mixture* (E–I states and Au foil, see text) and $\bar{F}_R^{th}(y, q)$ (full curve) for four scattering angles, $2\theta = 35.9^\circ$, 40.0°, 44.1° and 50.1°, are plotted in (a), (b), (c) and (d), respectively. The lower abscissa is the scaling variable, y, and the top abscissa the momentum transfer, q. In (a) and (b) the theoretical scaling function obtained from Young and Koppel model, $\bar{F}_{(YK)R}^{th}(y, q)$, is also plotted (short-dashed curve), while in (d) we include the asymptotic scaling function, $\bar{F}_R^{th}(y)$, (long-dashed curve).

motion which are lower than the molecular dissociation threshold, i.e. $\leqslant$4.75 eV. We note that this model treats the intramolecular scattering process in the framework of an ideal molecular rotation, decoupled from a purely harmonic molecular vibration and convoluted

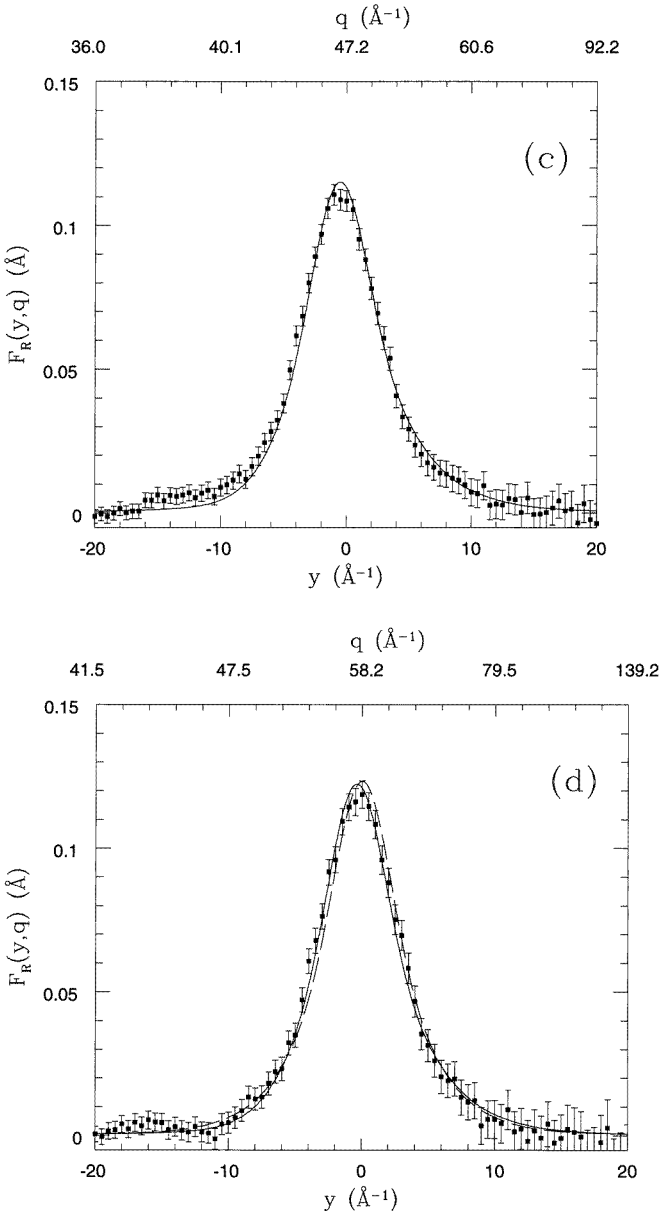

Figure 5. (Continued)

with the centre-of-mass momentum distribution scaling function. This model has been applied in previous papers to fluid and solid hydrogen for much lower values of q (i.e. $q < 20$ Å^{-1}) [26, 29]. The scaling function [12] calculated using this model has been subsequently convoluted with the proper resolution function $R(y)$ (see table 1) to yield the response function $\bar{F}^{th}_{(YK)R}(y, q)$ for *parahydrogen* (figures 3(a) and (b)) and for the *mixture* (figures 5(a) and (b)) for the low scattering angle detectors. The results of the Young and Koppel model are clearly worse than those obtained from the calculation presented

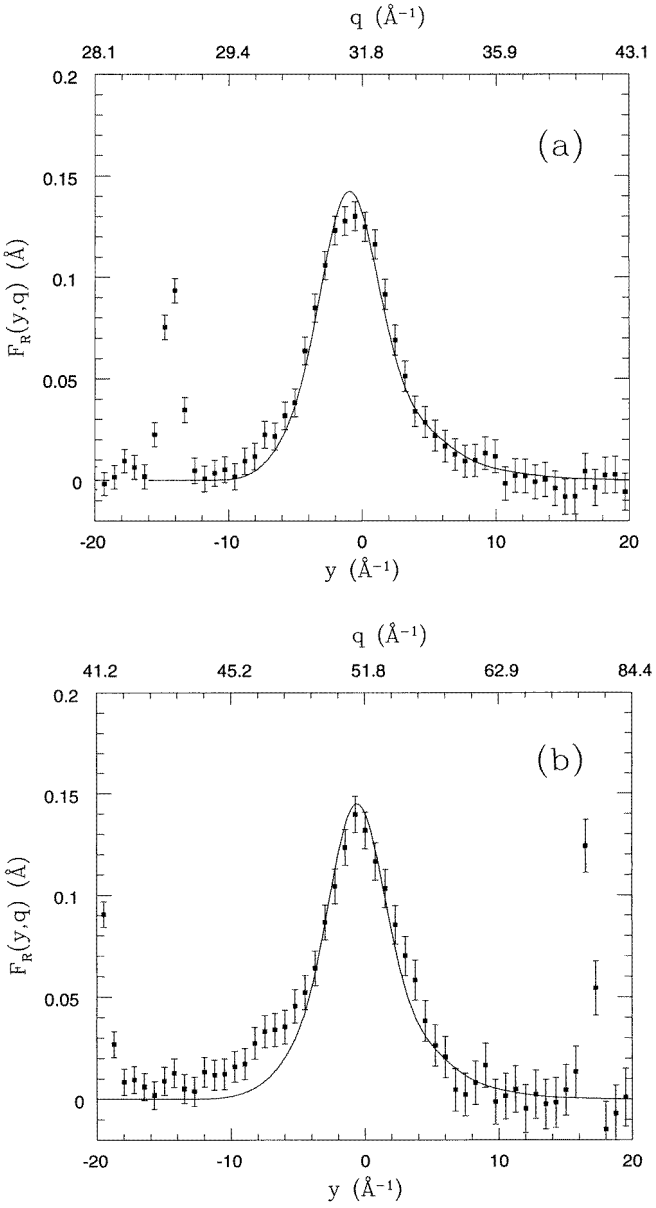

Figure 6. Experimental $F_R^{\exp}(y,q)$ (full squares) for *mixture* (E–I states and U foil, see text) and $\bar{F}_R^{th}(y,q)$ (full curve) for two scattering angles, $2\theta = 29.3^\circ$ and 42.4°, are plotted in (a) and (b), respectively. The lower abscissa is the scaling variable, y, and the top abscissa the momentum transfer, q. The spurious peaks are the cell contributions produced by two uranium resonances (left side 6671 meV, right side 20 872 meV).

in section 2, as also shown from the reduced χ^2 values reported in table 3, which get worse as q increases for the Young and Koppel model. A possible explanation of these results is that in DINS, even if the energy transfer to the internal degrees of freedom of the molecule does not exceed the molecular dissociation threshold (e.g., the energy transfer

to the internal motion corresponding to the peak position of figure 3(a) is $\cong$2.3 eV), the vibrational levels excited in the scattering process are probably affected by strong anharmonicities of the intramolecular potential. Moreover, as q increases the interaction between the rotational and vibrational levels becomes larger and larger with the consequent development of centrifugal distortions. For reduced q values ($q < 20$ Å^{-1}), these effects could be taken into account in an approximate way, by introducing some experimentally determined energy levels [12].

Let us briefly discuss our present calculation from the point of view of the roto-vibrational Young and Koppel model. Our corrected IA model contains two main approximations: (i) it assumes, as shown in section 2, that intramolecular final states are plane waves; (ii) it does not include any correlation between the difference of the rotational quantum numbers in the initial and final states Δj, and the total nuclear spin of the hydrogen molecule [4]. This second assumption is rigorous only for dissociated final states (owing to their infinite degeneracy in j). However, we believe that even for highly excited molecular bound states our description is quite reasonable because of the following facts: (i) the behaviour of these states, in the region where they overlap the initial ground state, is plane-wave like [19]; (ii) their density of states, i.e. the number of states in a unitary energy interval, is quite elevated owing to the anharmonic effects that reduce the gap between two subsequent vibrational states; and, in addition, because a large number of roto-vibrational states labelled with different rotational numbers are present [30].

Thus we think that our approximation is still valid for highly excited molecular bound states, even if they are not real plane waves and the j degeneracy does not hold rigorously.

5. Conclusions

In conclusion we have presented a model which uses centre of mass and internal momentum distributions as characteristic features of diatomic homonuclear molecules. Our model is able to offer a possible description of the main features of the experimental data at intermediate and high-q values, that is the shift of the recoiling peak and the overall shape of the scaling function, and has to be regarded as an improvement in the intermediate and high-q region with respect to the description of the scattering process of the Young and Koppel model. Our calculation does not appear to be completely satisfactory in reproducing the details and the line shape of the whole function, however this fact can be understood, owing to the approximations involved in the calculation and last but not least the present description in terms of plane waves of the wavefunction in the final state.

We can also conclude (see figures 1 and 2) that in our experiment INTERFSE are negligible as compared to INTRAFSE, since in any case the centre-of-mass motion represents a small contribution to the dynamics of the system. On the contrary INTRAFSE contribute significantly to the shape of the response function at q values $\leqslant$50 Å^{-1}. This is to our knowledge the first time that the relative weight of these two kinds of distinct FSE contributions has been discussed in a molecular fluid for these high-q values.

There is, however, an intrinsic limit of our theoretical calculation in its ability to describe the scattering at finite-q values from a single hydrogen molecule. In fact as we have pointed out in appendix A, it does not describe exactly the scattering process, since it does not fulfil the *incoherent sum rules for second and higher moments* of $F(y, q)$ (i.e. of $S(q, \omega)$) [11]. An exact calculation starting from a precise quantum mechanical treatment of the final state wavefunctions of a single molecule, i.e. dealing with the eigenstates of a realistic interatomic potential [30], is probably needed if one wants to obtain a further sensible improvement in the description of the experimental data.

Appendix

In this appendix we will briefly recall the idea proposed by Stringari [17] for taking into account in the inelastic structure factor an average value of the potential energy in the final states. Let us start from IA for the inelastic structure factor of a particle with mass M

$$S_{IA}(q,\omega) = \int n_i(\boldsymbol{p})\delta\left(\hbar\omega - \frac{\hbar^2(\boldsymbol{q}+\boldsymbol{p})^2}{2M} + \frac{\hbar^2 p^2}{2M}\right)\mathrm{d}\boldsymbol{p} \tag{38}$$

where $n_i(\boldsymbol{p})$ is the momentum distribution in the initial state. In this expression both the energies of the final and initial states have been assumed to be only kinetic. Stringari proposed to replace the initial kinetic energy with the exact value E_i of the total energy for the initial state, and to add a constant $\langle V_f\rangle$ in order to include the effect of the potential energy in the final states

$$S_{St}(q,\omega) = \int n_i(\boldsymbol{p})\delta\left(\hbar\omega - \frac{\hbar^2(\boldsymbol{q}+\boldsymbol{p})^2}{2M} - \langle V_f\rangle + E_i\right)\mathrm{d}\boldsymbol{p}. \tag{39}$$

The evaluation of the unknown quantity $\langle V_f\rangle$ can be performed using a well assessed sum rule, which holds exactly for both coherent and incoherent $S(q,\omega)$ [4]: the *first moment sum rule* for $S(q,\omega)$, that can be written as

$$\int_{-\infty}^{\infty}\omega S(q,\omega)\,\mathrm{d}\omega = \frac{\hbar q^2}{2M} \tag{40}$$

where $\hbar^2q^2/2M$ is the recoil energy of the struck particle. Substituting (39) in (40), the *first moment sum rule* appears as

$$\int_{-\infty}^{\infty}\omega\,\mathrm{d}\omega\int n_i(\boldsymbol{p})\delta\left(\hbar\omega - \frac{\hbar^2(\boldsymbol{q}+\boldsymbol{p})^2}{2M} - \langle V_f\rangle + E_i\right)\mathrm{d}\boldsymbol{p} = \frac{\hbar q^2}{2M}. \tag{41}$$

Using standard properties of $n_i(\boldsymbol{p})$ i.e. $\int n_i(\boldsymbol{p})\,\mathrm{d}\boldsymbol{p} = 1$, $\int n_i(\boldsymbol{p})\boldsymbol{p}\,\mathrm{d}\boldsymbol{p} = 0$ and $\int n_i(\boldsymbol{p})p^2\,\mathrm{d}\boldsymbol{p}$ $= (2M/\hbar^2)\langle T_i\rangle$ (where $\langle T_i\rangle$ is the mean value of the kinetic energy of the initial state), one obtains

$$\langle V_f\rangle = E_i - \langle T_i\rangle \equiv \langle V_i\rangle. \tag{42}$$

This result is quite important because it assesses that in this approximation the mean value of the potential energy is the same for both the initial and the final states. Introducing the previous relation into (39), one immediately obtains the Stringari approximation

$$S_{St}(q,\omega) = \int n_i(\boldsymbol{p})\delta\left(\hbar\omega - \frac{\hbar^2(\boldsymbol{q}+\boldsymbol{p})^2}{2M} + \langle T_i\rangle\right)\mathrm{d}\boldsymbol{p}. \tag{43}$$

Unfortunately, as pointed out by Rinat [31], Stringari's approximate description of FSE is biased by some defect. For instance it violates the *second moment sum rule*, that ought to hold exactly for incoherent $S(q,\omega)$. The incoherent limit of $S(q,\omega)$ is reached when $q \gg 2\pi/d$, where d is the typical spacing between the particles we are dealing with. It is generally accepted [11] that the incoherent limit is widely justified when $S(q) = \int_{-\infty}^{\infty} S(q,\omega)\,\mathrm{d}\omega \simeq 1$. This relation, which is known as incoherent *zeroth moment sum rule*, is fulfilled in the case of hydrogen for $q > 20$ Å^{-1} where ($|S(q)-1| \leqslant 3.1\times10^{-3}$) [32]. The *second moment sum rule* for incoherent $S(q,\omega)$ can be written as

$$\int_{-\infty}^{\infty}\left(\omega - \frac{\hbar q^2}{2M}\right)^2 S(q,\omega)\,\mathrm{d}\omega = \frac{2\langle T_i\rangle}{3M}q^2. \tag{44}$$

Introducing (39) into the previous equation and using the aforementioned properties of $n_i(\boldsymbol{p})$, one obtains

$$\frac{2\langle T_i\rangle}{3M}q^2 - \left(\frac{\langle T_i\rangle^2}{\overline{h}^2} - \frac{\overline{h}^2\langle p^4\rangle}{4M^2}\right) = \frac{2\langle T_i\rangle}{3M}q^2. \tag{45}$$

This relation is clearly false for a generic $n_i(\boldsymbol{p})$ (e.g., for a Gaussian shape of the momentum distribution, the terms within brackets in (45), become: $(\overline{h}^2/4M^2)\ (\langle p^2\rangle^2 - \langle p^4\rangle) = (3\overline{h}^2/4M^2)\ \langle p^2\rangle^2 \neq 0$); but for $q^2 \gg \langle p^2\rangle$, the difference between the right- and the left-hand side of (45) becomes less and less relevant. In the limit of $q \to \infty$, the Stringari approximation reproduces IA, and the *second moment sum rule* is recovered exactly.

References

[1] Mayers J and Evans A C 1994 *Nuovo Cimento* **16** 737
[2] Lam L and Platzmann P M 1974 *Phys. Rev.* B **9** 5122
Bauer G E and Schneider J R 1983 *Phys. Rev. Lett.* **52** 2061
[3] West G B 1975 *Phys. Rep.* **18** 263
Ciofi degli Atti C, Pace E and Salmè G 1991 *Phys. Rev.* C **43** 1155
[4] Lovesey S W 1987 *Theory of Neutron Scattering from Condensed Matter* vol 1 (London: Oxford University Press)
Hohenberg P C and Platzmann P M 1966 *Phys. Rev.* **152** 198
[5] Pace E, Salmè G and West G B 1991 *Phys. Lett.* **273B** 205
[6] Pace E, Salmè G and Rinat A S 1994 *Nucl. Phys.* A **572** 1
[7] Watson G I 1996 *J. Phys.: Condens. Matter* **8** 5955
[8] Andreani C and Dore J 1991 *Rep. Prog. Phys.* **54** 731
[9] Mayers J 1993 *Phys. Rev. Lett.* **71** 1553
[10] Andreani C, Filabozzi A and Pace E 1995 *Phys. Rev.* B **51** 8854
[11] Sears V F 1984 *Phys. Rev.* B **30** 44
Silver R N 1988 *Phys. Rev.* B **37** 3794
Glyde H R 1994 *Phys. Rev.* B **50** 6726
[12] Bafile U, Zoppi M, Celli M, Magli R, Evans A C and Mayers J 1996 *Physica* B **226** 304
[13] Young J A and Koppel J U 1964 *Phys. Rev.* A **135** 603
[14] Andreani C, Filabozzi A, Mayers J and Pace E 1996 *Phys. Rev.* B **54** 9
[15] Colognesi D and Pace E 1997 Deep inelastic neutron scattering from diatomic molecules *Phys. Rev.* B submitted
[16] Andreani C, Colognesi D, Filabozzi A, Nardone M and Pace E 1997 *Physica* B **234–236** 329
[17] Stringari S 1987 *Phys. Rev.* B **35** 2038
[18] Sears V F 1985 *Can. J. Phys.* **63** 68
[19] Gunn J M F, Andreani C and Mayers J 1986 *J. Phys. C: Solid State Phys.* **19** 835
[20] Bransden B H and Joachain C J 1983 *Physics of Atoms and Molecules* (Harlow: Longman Scientific and Technical)
[21] Evans A C, Mayers J, Timms D N and Cooper M J 1993 *Z. Naturf.* a **48** 425
Loong C K, Ikeda S and Carpenter J M 1987 *Nucl. Instrum. Methods* A **260** 381
[22] Mughabghab S F, Divadeenam M and Holden N E 1981 and 1984 *Neutron Cross Sections* vol I, parts A and B (New York: Academic)
[23] Seeger P A, Taylor A D and Brugger R M 1985 *Nucl. Instrum. Methods* A **240** 98
[24] Timms D N, Evans A C, Boninsegni M, Ceperley D M, Mayers J and Simmons R O 1996 *J. Phys.: Condens. Matter* **8** 6665
[25] Silvera I S 1980 *Rev. Mod. Phys.* **52** 393
[26] Andreani C, Colognesi D, Filabozzi A, Nardone M and Azuah R T 1997 *Europhys. Lett.* **37** 329
[27] Ceperley D M 1995 *Rev. Mod. Phys.* **67** 279
[28] Wagner M and Ceperley D M 1994 *J. Low Temp. Phys.* **94** 161
[29] Langel W, Price D L, Simmons R O and Sokol P E 1988 *Phys. Rev.* B **38** 11 275
Herwig K W, Gavilano J L, Schmidt M C and Simmons R O 1990 *Phys. Rev.* B **41** 96
[30] van Kranendonk J 1983 *Solid Hydrogen* (New York: Plenum)
[31] Rinat A S 1987 *Phys. Rev.* B **36** 5171
[32] Zoppi M 1993 *Physica* B **183** 235